DOI: 10.24352/UB.OVGU-2017-012 TECHNISCHE MECHANIK, 36, 1-2, (2016), 88 - 101
submitted: July 27, 2015

A Robust, Compressible, Hyperelastic Constitutive Model for the Mechanical Response of Foamed Rubber

M. Lewis

An overview of the roles that cellular elastomers play in engineered systems and the phenomenology of these materials is presented. Available data on these materials and empirical modeling approaches that have been used to approximate the mechanical response of these materials is then considered. The Compressible, Hyperelastic, Isotropic, Porosity-based Foam model (CHIPFoam), a model developed at Los Alamos National Laboratory (LANL) with a simple micromechanical basis, is then described, and its ability to fit available data is demonstrated. Finally, extensions and improvements to the model and the additional predictivity to be achieved with these extensions are discussed.

1 Introduction

Cellular solids are both useful and common in everyday applications ranging from baked bread to impact absorbers. These materials are used in engineered systems. Specifically, cellular polydimethylsiloxane (PDMS) with different fillers in either a blown foam form (room temperature vulcanized or RTV) or in a leached foam form (cellular silicone or CS) is often used in cushions and pads in engineered systems. These foams are often the most compliant materials used in such systems. As a result, displacements of and stresses in neighboring components are strongly affected by the thermomechanical behavior of these materials.

PDMS is a silicon-based polymer. These filled PDMS materials are in the rubbery regime, well above their glass transition temperatures, over a large temperature range. In this regime, the materials can sustain large elastic strains. This feature puts these materials in the class of materials that must be modeled with hyperelastic models. Hyperelastic models are described in terms of strain energy functions from which stress states are derived. These strain energy functions are analogous to potential functions in three-dimensional space, such as gravity potential or electrostatic potential fields, whose gradients in their respective function spaces produce conjugate forces (gravitational or electromotive in these cases).

Solid elastomers are often idealized as incompressible. This is because their bulk moduli are typically two to four orders of magnitude larger than their shear moduli for small strain response. Unlike solid elastomers, foamed rubber is initially quite compressible because of its porosity, so most of the strain energy functions used for solid elastomers are not appropriate for foamed elastomers.

Our ability to model these materials has been poor until very recently. Despite attempts to model foam structures using representative volume element (RVE) approaches like those used by Hohe and Becker (2003) and Bardenhagen *et al.* (2005), the only model for this class of materials that reproduced the limited extant test data had no basis in actual foam mechanics and, as such, could not be applied to predict the response of foams with different porosities or relative densities based on data from foams of known porosities or relative densities. We propose a model that has a basis in the response of an isolated pore in a Neo-Hookean solid that addresses this deficiency and has been applied to represent foam components with varying porosities. In the current paper, the basis of the Compressible, Hyperelastic, Isotropic, Porosity-based Foam model (CHIPFoam) developed by Lewis and Rangaswamy (2015) is described and corrected, and its applicability for relevant materials is demonstrated.

In the next section of this paper, Phenomenology, the phenomenology of elastomeric foams in general and some of the issues in obtaining data from thin foam samples are described. Following that, a quick review of hyperelasticity is presented, and the previously used model, Hyperfoam, is described and discussed, along with issues associated with its use for our components in the Hyperfoam section. In the CHIPFoam Basis section, the basis for the CHIPFoam model is presented, and the purpose of each term in the strain energy is explained. Additionally, cases when some of the terms may be omitted are identified.

The process for fitting available data is described in the Data Fitting section, along with examples of a fit to data from a near uniaxial strain test. The model implementation as a UHYPER subroutine in ABAQUS is presented in the Model Implementation section. Finally, recommendations for improvements to the modeling of these materials are presented in the Further Work section of this paper.

2 Phenomenology

2.1 Nonlinearity and Dependence on Porosity

As mentioned previously, the mechanical response of foamed elastomers is nonlinear and very dependent on the porosity of the foam. The porosity is directly related to the foam density as follows:

$$\varphi_o = 1 - s \equiv 1 - \rho_r = 1 - \frac{\rho_f}{\rho_s} \ , \tag{1}$$

where ϕ_o is the porosity of the foam, s is the solidity of the foam, ρ_r is the relative density of the foam, ρ_f is the mass density of the foam, and ρ_s is the mass density of the parent material. The nonlinearity of the foams uniaxial mechanical response is demonstrated in Figure 1, as is the strong dependence of the mechanical response on the porosity of the material.

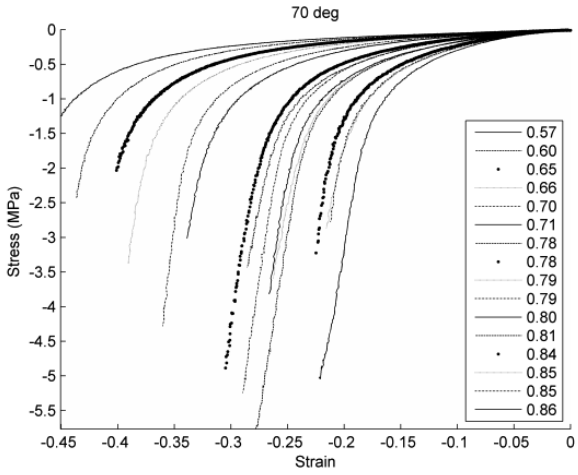

Figure 1. Engineering stress vs. engineering strain loading curves from uniaxial compression tests of cushion material of densities ranging from 0.57 g/cc to 0.86 g/cc at 70°C. Note that compressive quantities are plotted as negative in this figure. The plot demonstrates the nonlinear mechanical response seen in these foams and the strong dependence of this response on the density of the foams, which is directly related to the foam porosity by equation (1).

2.2 Mullins Effect, Hysteresis, and Large Deformation Elasticity

Additional mechanical phenomena are seen in these materials when they are cycled in compression. Figure 2 shows the resulting stress-strain behavior when a material with an estimated porosity somewhere between 20% and 25% is cycled to nearly 20% strain in compression four times. The first cycle loading curve stresses lie above the loading curve stresses for subsequent cycles, which all tend to overlay each other. This effect, a cyclic softening of the loading curve, is known in the elastomer literature as the Mullins effect (Mullins, 1948), after Leonard Mullins, a rubber researcher the mid-20th century.

The unloading curve stresses in Figure 2 are nearly identical from one cycle to the next and all are lower than the loading cycle stresses at the same strains. This mechanical hysteresis is typically observed in elastomers.

An additional feature of the curves shown in Figure 2 is that the curves unload and recover to a strain near zero at

zero stress, indicating that the large deformation (nearly 20% strain) is almost completely recoverable. In order to model this phenomenology, a theory capable of handling large elastic strains is needed.

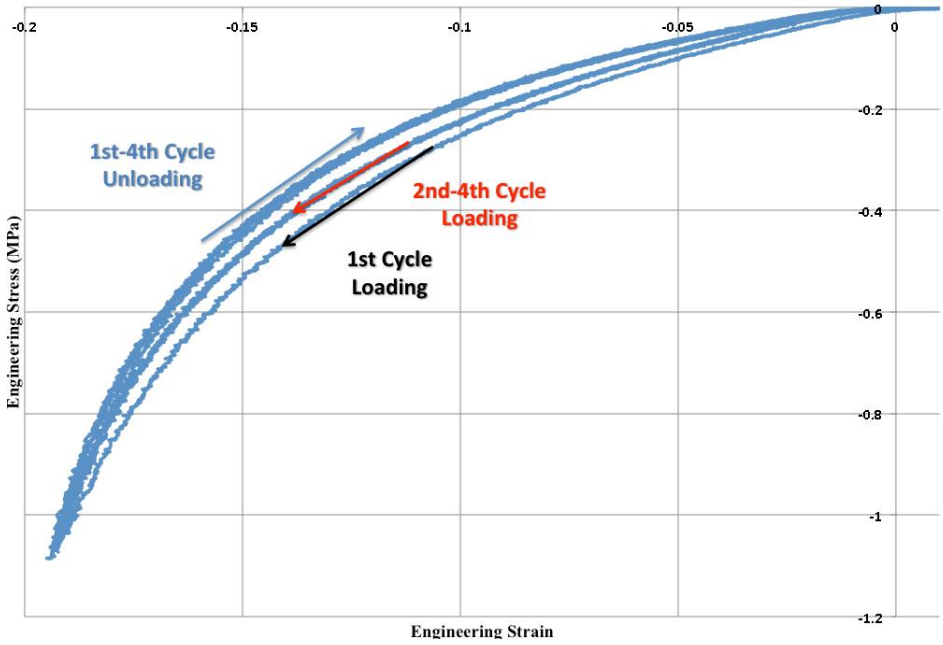

Figure 2. Cyclic engineering stress vs. engineering strain curves from uniaxial compression tests of a cushion material at 20°C. Hysteresis is apparent in that the unloading of the specimen occurs at stresses lower than those seen in loading. Mechanical energy is being dissipated. Also, the difference between the first cycle loading curve and subsequent cycle loading curves is evidence of the Mullins effect, a cyclic softening phenomenon.

2.3 State of Stress and Strain in Thin Specimens

While the data presented in Figures 1 and 2 are reported as axial stress and strain from compression tests, it should be noted that they are not from uniaxial stress tests. The thicknesses of these specimens were approximately 1 mm, while the diameter of the specimens were approximately 16 mm. As the platens in these tests were not lubricated and the specimen lateral strain was not measured, it is reasonable to assume that the strain state most nearly approximated uniaxial strain, and that lateral strains were zero while radial stresses in the specimen were probably not negligible.

An additional issue is that many of these materials have "skins," or regions of very low porosity near free surfaces. As a result, stress cushions have more of a sandwich composite structure. For the present time we ignore this effect, though finite element modeling techniques for modeling this sort of foam core structure are available.

2.4 Low Strain Behavior in Compression under Near-Uniaxial Stress Conditions

A compression test was conducted on a sample of S5370, a blown PDMS foam, at LANL. In the test, the platen-sample interfaces were lubricated and lateral strain was manually measured with a micrometer. The observed sample lateral strain was not linear in the applied axial strain, and a plot showing the large strain Poisson's ratio and the decrease in relative volume vs. axial compressive strain (shown as positive in compression) is presented in Figure 3, with an accompanying stress-strain curve shown in Figure 4.

The large strain Poisson's ratio used is defined as follows:

$$\nu_{NL} \equiv \frac{-e_l}{e_a} \ , \tag{2}$$

where ν_{NL} is the large strain Poisson's ratio, e_l is the engineering lateral strain, and e_a is the engineering axial strain in a sample subjected to uniaxial stress. Additionally, the relative volume is defined as the ratio of the initial density to the current density of the sample at a point of interest, typically the gauge section.

The decrease in Poisson's ratio is typically associated with an inflection point in the stress-strain curve and both are thought to be a consequence of buckling in the foam.

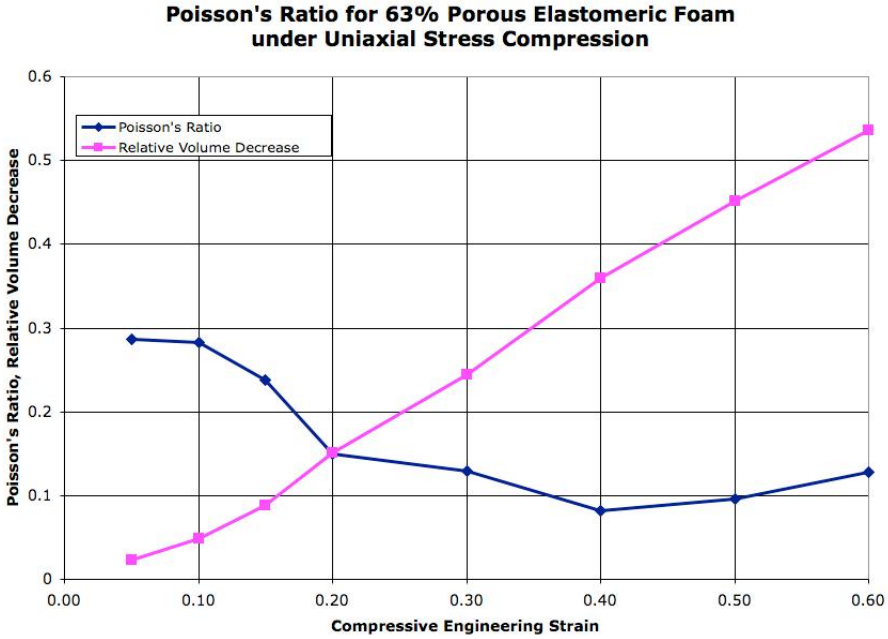

Figure. 3. Measured large strain Poisson's ratio and relative volume decrease in a lubricated S5370 (blown PDMS foam) specimen as a function of axial engineering strain, shown positive in compression. Note the drop in Poisson's ratio early in compression, thought to be associated with hyperelastic buckling in the foam structure in foams of low relative density or high porosity. It is often associated with an inflection point in the stress-strain curve, as indicated in Figure 4.

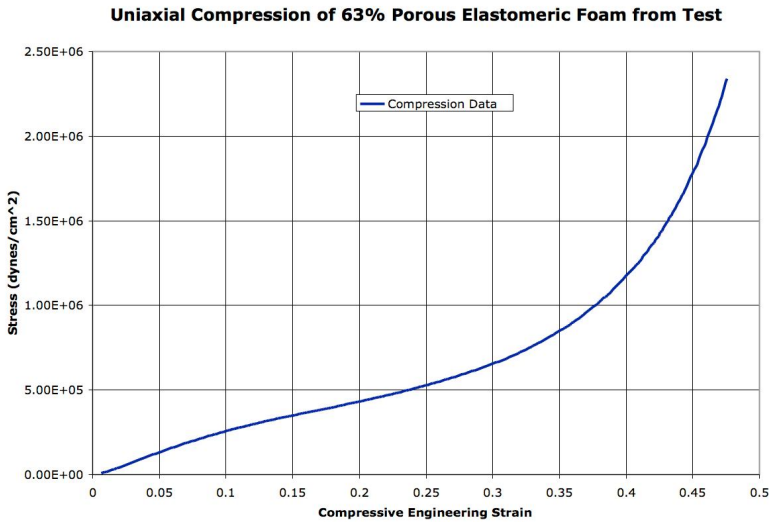

Figure 4. Loading stress-strain curve for an S5370 (blown PDMS foam) specimen in compression. Compressive quantities are shown as positive. Note an inflection point in the curve near an engineering strain of 0.1, near the strain at which the Poisson's ratio data shown in Figure 3 begins to decrease.

2.5 Viscoelasticity and Temperature Effects

It is well known that stress cushion materials exhibit stress relaxation and other viscoelastic phenomena. These phenomena are effected by temperature in that increasing temperature tends to decrease relaxation times. Some work on characterizing and modeling such behavior is described by Yang *et al.* (2000). Additionally, work by Treloar (1958) has demonstrated that the shear stiffness of rubber is strongly dependent on temperature, and is characteristically linear in absolute temperature, i.e. increasing in stiffness as temperature is raised.

3 Hyperfoam

It is clear that the mechanical behavior of elastomeric foams is complicated. While the Mullins effect, hysteresis, and other dissipative phenomena like viscoelasticity and potential gas flow effects are important parts of that behavior, a crucial part of the response is large deformation elasticity. In order for a mechanical constitutive theory for these materials to be useful over a large set of possible strain histories, it must be based on hyperelastic theory.

3.1 A Brief Review of Hyperelastic Theory

Hyperelastic theory is based on the existence of a strain energy density function, W, that is computable for each strain state. The strain measures used are appropriate for large elastic strain. The strain energy density is the work required/ per unit initial material volume, to reach the strain state. Through work and energy arguments, one can show that the Cauchy stress may be computed from the strain energy function as follows:

$$\boldsymbol{\sigma} = \frac{1}{J}\frac{\partial W}{\partial \mathbf{F}} \cdot \mathbf{F}^T \ , \tag{3}$$

where $\boldsymbol{\sigma}$ is the Cauchy stress tensor, J is the relative volume, and $\mathbf{F}$ is the deformation gradient, or the gradient of the current location of each point with respect to the original configuration, or

$$\mathbf{F} \equiv \frac{\partial \mathbf{x}}{\partial \mathbf{X}} \ , \tag{4}$$

where $\mathbf{x}$ is the vector to a point in the current configuration and $\mathbf{X}$ is the vector to that point in the initial configuration. A superscript T indicates the transpose of a tensor.

W may be expressed as a function of invariants of the Cauchy-Green tensors or in terms of principal stretches, as Ogden argues for. Typical invariants used for strain energy functions are J, $\bar{I}_1$, and $\bar{I}_2$. J has already been defined but can also be calculated as the determinant of $\boldsymbol{F}$. $\bar{I}_1$ is the trace of the isochoric Cauchy-Green tensor (either left or right), as follows:

$$\bar{I}_1 \equiv Tr\left(\overline{\mathbf{B}}\right) = Tr\left(J^{-2/3}\mathbf{F}\cdot\mathbf{F}^T\right). \tag{5}$$

Although we will not use it here, it is worth mentioning that $\bar{I}_2$ is the trace of the inverse of the isochoric Cauchy-Green tensor.

It is relatively easy to show that the Cauchy stress for a material with a strain energy function expressed as a function of J and $\bar{I}_1$ is as follows:

$$\boldsymbol{\sigma} = \frac{2}{J}\frac{\partial W}{\partial \bar{I}_1} dev\left(\overline{\mathbf{B}}\right) + \frac{\partial W}{\partial J}\mathbf{i} = \frac{2}{J}\frac{\partial W}{\partial \bar{I}_1}\left(\overline{\mathbf{B}} - \frac{\bar{I}}{3}\mathbf{i}\right) + \frac{\partial W}{\partial J}\mathbf{i} \ , \tag{6}$$

where **i** is the second order identity tensor.

Similarly, for cases where the strain energy function is expressed in terms of principal stretches, λ_i, and J, as in the case of the Hyperfoam model, the Cauchy stress can be shown to be as follows:

$$\boldsymbol{\sigma} = \frac{1}{J}\sum_{i=1}^{3}\lambda_i \frac{\partial W}{\partial \lambda_i}\mathbf{p}_i \otimes \mathbf{p}_i + \frac{\partial W}{\partial J}\mathbf{i} \ , \tag{7}$$

where $\mathbf{p}_i$ are the principal directions associated with the principal stretches.

W has additional requirements of convexity in the space of the deformation gradient, but these are beyond the scope of the current paper.

3.2 Hyperfoam Model Form

The Hyperfoam model is a variation on an Ogden (1984) strain energy function proposed by Jemiolo and Turtletaub (2000), who moved from the isochoric principal stretches used by Ogden to the full principal stretches. The strain energy function for the Hyperfoam model is in terms of principal stretches and J and is as follows:

$$W_H = \sum_{i=1}^{N}\frac{2\mu_i}{\alpha_i^2}\left[\lambda_1^{\alpha_i} + \lambda_2^{\alpha_i} + \lambda_3^{\alpha_i} + \frac{1}{\beta_i}\left(J^{-\alpha_i\beta_i} - 1\right)\right]. \tag{8}$$

The exponents in equation (8) are typically not whole numbers and may be either positive or negative. The Hyperfoam model reproduces test data well, provided the right test data are available. As mentioned previously, available test data are often best characterized as uniaxial strain compression data. As a result, it is not possible to differentiate between the contribution of the axial principal strain term and that of the relative volume term in the strain energy function.

Fitting Hyperfoam typically involves using a nonlinear least squares method, usually inside ABAQUS, and the resulting model parameters have no discernible physical association. When data are modified slightly, the model parameters can change substantially. Additionally, as available data are from tests which approximate uniaxial strain compression conditions, it is common to set the Poisson's ratio to zero to disambiguate the effects of the principal strain and relative volume terms.

While this approach is a way to use available data, it artificially turns uniaxial strain data into uniaxial stress data and ignores the effects of variable Poisson's ratio seen in Figure 3. One would expect that as a foamed rubber is consolidated in one direction, that its response in transverse directions would stiffen. Using a zero Poisson's ratio decouples the responses in orthogonal directions very effectively and prevents this expected stiffening phenomenon.

4 CHIP Foam basis

The reader should be convinced of the many shortcomings of the Hyperfoam model at this point. This next section describes the fundamental basis of the CHIPFoam model, which was developed to have a micromechanical basis and be predictive of the response of foams with various porosities. CHIPFoam is, as the acronym indicates, an isotropic, hyperelastic model that includes compressibility effects, both in terms of the foam as a material and the parent material compressibility as well.

The model consists of four components. First, a smaller deformation component which attempts to capture small strain linear behavior and buckling-type behavior within the foam is included. This term includes uncoupled

deviatoric or shear and volumetric parts. Next, a term that captures the response of an incompressible spherical shell is used to describe the stiffening at large deformations. This term couples deviatoric and volumetric behaviors. A third term accounts for matrix compressibility to allow a consistent response at large compressions. Finally, an optional term which is somewhat coupled with the second third terms can be included to represent the effect of gas compression in closed cell foams. For most of our applications, this term and its complications can be ignored.

4.1 Smaller Strain Compressive Behavior Including Buckling Effects

To capture smaller strain near linear behavior, a simple Neo-Hookean strain energy function for shear response is introduced. An accompanying volumetric strain energy function is added to include initial compressibility of the foam. It is quadratic in *J*. This early part of the strain energy function is as follows:

$$W_L = \frac{\hat{G}}{2}\left(\bar{I}_1 - 3\right) + \frac{\hat{K}}{2}\left(J-1\right)^2 . \tag{9}$$

This strain energy function provides small strain behavior that linearizes to infinitesimal strain linear elasticity with shear and bulk moduli of $\hat{G}$ and $\hat{K}$.

In order to capture a decreasing Poisson's ratio and buckling behavior, the volumetric strain energy function has been modified to instantaneously change from quadratic to linear at a predefine relative volume, as follows:

$$\begin{aligned} W_{LB} = {} & \frac{\hat{G}}{2}\left(\bar{I}_1 - 3\right) \\ & + \hat{K}\left\{\left(J_b - 1\right)\left(J - \frac{J_b+1}{2}\right) + \mathrm{H}\left[J - J_b\right]\left[\frac{\left(J-1\right)^2}{2} - \left(J_b - 1\right)\left(J - \frac{J_b+1}{2}\right)\right]\right\} \end{aligned} \tag{10}$$

The expression $\mathrm{H}\left[J - J_b\right]$ in equation (10) is the Heaviside step function, equal to zero for negative arguments and unity for nonnegative arguments. While equation (10) is not strictly convex in *J,* terms to be added later will guarantee convexity of the total strain energy function in *J*.

A plot of the large strain Poisson's ratio as defined in (2) is presented in Figure 5 for the strain energy function of equation (9) and that of equation (10) with shear to bulk modulus ratio of 0.6 and a value of J_b, the buckling relative volume, of 0.94.

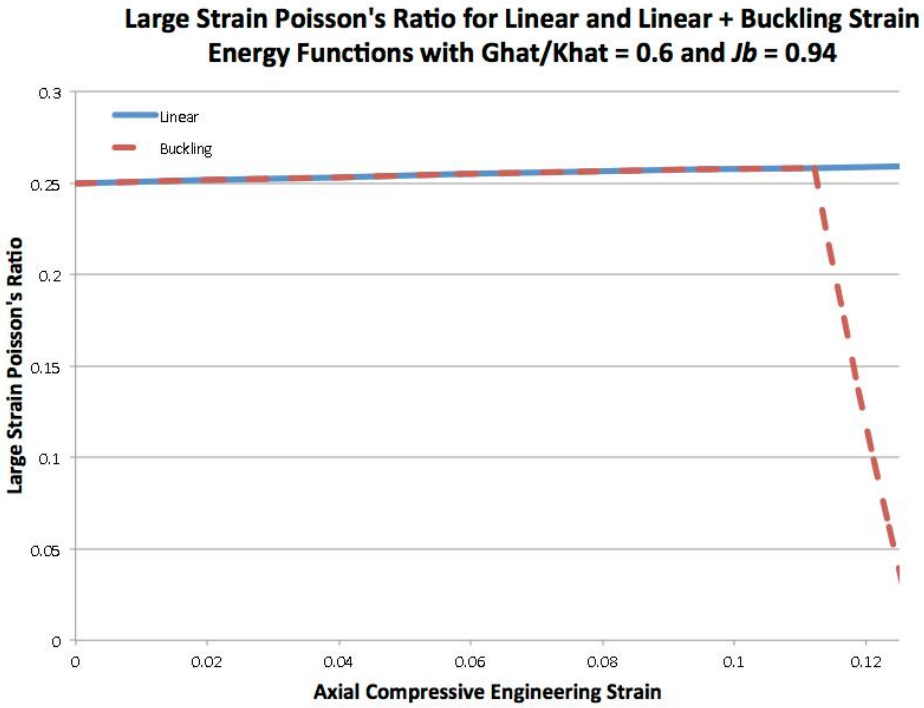

Figure 5. A plot of the large strain Poisson's ratio as defined in (2) for the strain energy functions of equations (9) and (10) demonstrating the drop achievable with the buckling modification presented in equation (10). Note that a ratio of shear to bulk modulus of 0.6 was used to provide an initial Poisson's ratio of 0.25 and a volumetric buckling relative volume of 0.94 was chosen.

It should be noted that the modification of the volumetric term presented in equation (10) is in no means the only modification acceptable or useful. Instead of transitioning to an essentially zero bulk tangent modulus, one could transition to different tangent bulk moduli at different points using sets of tangent parabolas at specified relative volumes. Such an approach would allow for near exact matches of Poisson's ratios, although the challenge of coding necessary to support this in a material model is probably not justified by these gains in fidelity.

4.2 Pore Mechanics Basis and Strain Energy Function

In order to capture the stiffening behavior seen as a foamed rubber is compressed to a relative volume approaching the solidity of the material, the response of the simplest possible isotropic Representative Volume Element (RVE), a spherical shell of incompressible rubber, is considered. If the ratio of inner radius to outer radius is chosen to provide the right solidity of the volume inside the outer boundary of the sphere, then this RVE has the same initial porosity as the foam, the only material structure statistic that is reproduced with this RVE choice. As this particular RVE choice is so simple, and does not capture spatially varying or relevant length scales, it is more appropriate to refer to it as a mechanical surrogate. This approach is somewhat similar tot that taken by Dienes and Solem (1999) for the response of a void in a linear elastic material.

By invoking symmetry and incompressibility, one can solve for the displacement field inside this surrogate shell subjected to uniform radial compression on its boundary followed by a volume conserving stretch field superposed on the entire compacted shell. Once the kinematics have been solved, one can then use a strain energy function for the parent material and integrate the strain energy density over the entire initial volume of material, normalize it by the initial volume enclosed by the outer boundary of the shell, and calculate a strain energy function appropriate for this simplest of micromechanical models. We initially assumed a parent material with a Mooney-Rivlin strain energy function, linear in both the first and second isochoric invariants. The resulting strain energy function is published (Lewis and Rangaswamy, 2011). The generality added by the inclusion of the second invariant was not necessary for good data fits, so the strain energy was simplified to include only a Neo-Hookean parent material. The resulting strain energy function term is as follows:

$$W_D = C_{10}\left[\bar{I}_1 f\left(J,\phi_o\right) - 3\left(1-\phi_o\right)\right], \tag{11}$$

where the function multiplying the first isochoric invariant is as follows:

$$f\left(J,\phi_o\right) = \frac{2J-1}{J^{1/3}} + \left(2-2J-\phi_o\right)\left[\frac{\phi_o}{J-\left(1-\phi_o\right)}\right]^{1/3}, \tag{12}$$

and ϕ_o is the initial porosity or void volume fraction of the material.

We have chosen to refer to the strain energy function (11) as the Danielsson function, after Mats Danielsson et al. (2004), who published a version of it in 2004, although it was not expressed in invariant form as shown here. The Danielsson function explicitly couples volumetric and shear response. This leads to shear stiffening response with compression in addition to the volumetric stiffening expected. It should be noted that the Danielsson strain energy function loses polyconvexity if the initial porosity is greater than 0.71 and the applied relative volume is approximately 0.4 or less. For the foams we have been interested in modeling thus far, the initial porosities have been substantially less than this limiting porosity.

Note that this function has a singularity as the relative volume approaches the solidity of the material. This is sensible in that the derivation of the Danielsson function involves the assumption of incompressibility in the parent material. This is good if one is trying to model conditions of true "lock-up" in the material, however it is problematic for real finite element analyses. During an implicit solution calculation in a finite element analysis, many trial states may be passed to a material model subroutine. The likelihood of the subroutine receiving a value of J that is less than the initial solidity of the material is high unless the entire analysis involves uniform low strains.

A plot of the function f is shown in Figure 6 for a material with a porosity of 0.52.

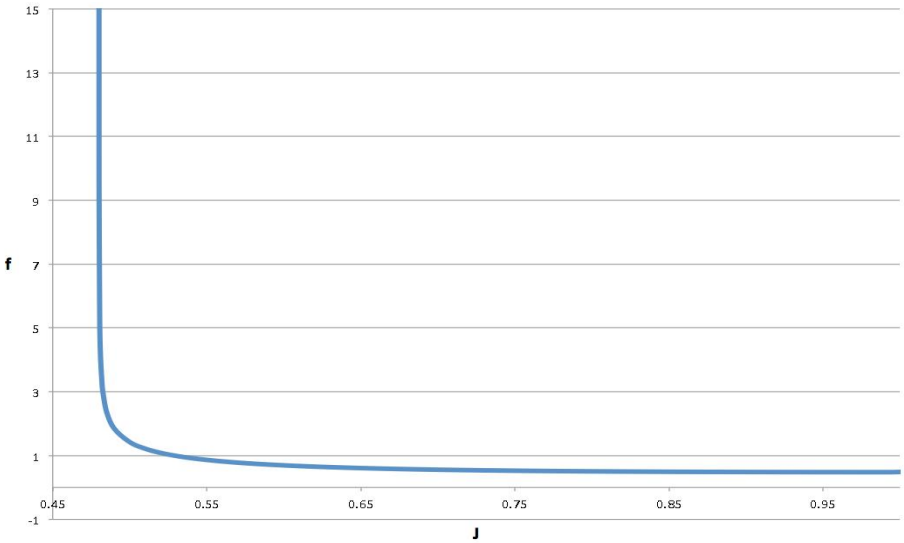

Figure 6. The function f of J in (12) for a material with a porosity of 0.52. The singular behavior discussed in the text is clearly demonstrated.

4.3 Parent Material Compressibility Effects to Remove Singular Behavior

In order to avoid the singularity problem mentioned in the previous section, it was necessary to consider compressibility of the parent material. Rather than do this in an *ad hoc* manner, the problem of compression of the spherical shell assuming a compressible parent material was attempted. That problem was not found to be tractable. An approximation is possible, however and is described here. More detail is available in Lewis and Rangaswamy (2013).

The first observation to make is that in the compression of a spherical shell of an incompressible material, only the deviatoric stresses are directly computable from the constitutive model. The pressure field must be solved for to satisfy equilibrium and boundary conditions. The pressure field was solved for and it was found that it could be reasonably approximated (Lewis and Rangaswamy, 2013) as a constant pressure in the spherical shell as follows:

$$\widetilde{p} = p_g + C_{10}\left[\frac{\varphi_o^{1/3}\left(4J-4+5\varphi_o\right)}{\left(J-1+\varphi_o\right)^{4/3}} - \frac{\left(4J-1\right)\left(4J+1\right)}{3J^{4/3}}\right], \tag{13}$$

where p_g is the pressure in the interior of the pore, potentially from any gas present.

The effect of a uniform pressure in a compressible shell is simple to calculate and is to uniformly compact the entire shell. For tractability, a compressibility model for the parent material that leads to a logarithmic relation between relative volume of the material and the pressure was assumed. This implies a volumetric strain energy function for the parent material as follows:

$$W = K\left(J_m \ln J_m - J_m + 1\right), \tag{14}$$

where J_m is the relative volume in the parent material and K is the apparent bulk modulus of the parent material. The solution for J_m is necessary for this part of the strain energy function, and is simply as follows:

$$J_m = e^{-\widetilde{p}/K} . \tag{15}$$

All of the previous suggests that some modifications need to be made to the Danielsson function to be compatible with the assumption of parent material compressibility. It is appropriate and necessary to decompose the macroscopic relative volume into two parts, namely a part due to the incompressible response of the material in the RVE and a part due to the parent material compressibility. The appropriate decomposition is a multiplicative one as follows:

$$J = \bar{J} J_m . \tag{16}$$

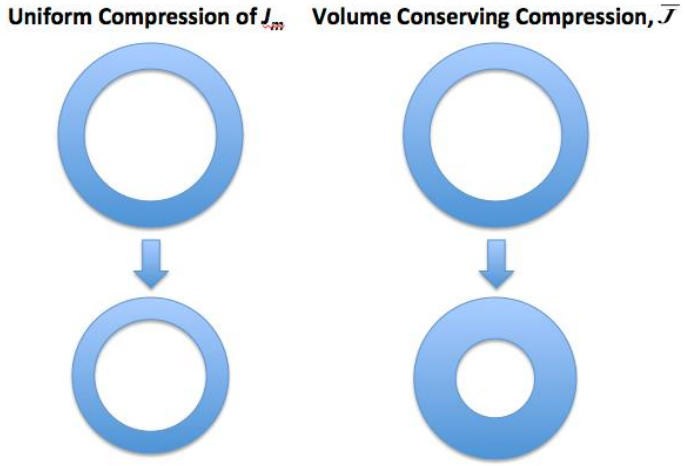

Figure 7. Schematics of the compressive deformations associated with J_m (left) and $\bar{J}$ (right).

J_m is as in (15), but the pressure is now

$$\widetilde{p} = p_g + C_{10}\left[\frac{\varphi_o^{1/3}\left(4\bar{J}-4+5\varphi_o\right)}{\left(\bar{J}-1+\varphi_o\right)^{4/3}} - \frac{\left(4\bar{J}-1\right)\left(4\bar{J}+1\right)}{3\bar{J}^{4/3}}\right], \tag{17}$$

consistent with the original derivation. Note that $\bar{J}$ has a physical lower limit of the solidity of the material, s.

The Danielsson function must be modified similarly to be consistent with this parent material compressibility inclusion. The modified Danielsson function is as follows:

$$W_D^C = C_{10}\left\{ J_m\left[\bar{I}_1 f\left(\bar{J},\varphi_o\right) - 3\left(1-\varphi_o\right)\right] - J\left(\bar{I}_1 - 3\right)\left(1-\varphi_o\right)\left.\frac{d\bar{J}}{dJ}\right|_{\bar{J}=1} \right\}. \tag{18}$$

Note that equation (18) is modified from what appears in Lewis and Rangaswamy (2015), to meet requirements that the pressure be zero when the relative volume is unity. The energy stored in the compression of the parent material is as follows:

$$W_m = \left(1-\phi_o\right) K\left(J_m \ln J_m - J_m + 1\right). \tag{19}$$

4.4 Effect of Gas Pressure in Voids

Equations (13) and (17) explicitly contain a gas pressure term. In order to capture that term properly and also include a gas compression term in the strain energy function to represent energy stored in the gas in closed cell foams or under loading conditions that are rapid enough that the gas cannot escape, it is necessary to consider the behavior of gas trapped in the inner cavity of the spherical shell. It should be noted that for many of our conditions these gas terms may be neglected. For completeness they are presented here.

For our purposes and to be consistent with zero energy at a reference state with a nonzero absolute pressure, we formulate the gas pressure as a function of the relative volume of the gas as follows:

$$p_g = p_o\left(J_g^{-\gamma} - 1\right), \tag{20}$$

where p_o is the ambient pressure, J_g is the relative volume of the gas, and γ is an exponent that may be chosen as unity for isothermal deformations and as the ratio of the gas specific heats at constant pressure and constant volume for adiabatic deformations. A strain energy function, then, for the gas is obtained by integrating the pressure with respect to the relative volume with a negative sign applied for thermodynamic consistency. We then scale the resulting strain energy function by the initial volume of the inner cavity as follows:

$$W_g = p_o\phi_o \times \begin{cases} J_g - \ln\left(J_g\right) - 1 & \textit{isothermal} \\ J_g - \dfrac{1}{\gamma-1}\left(\gamma - J_g^{1-\gamma}\right) & \textit{adiabatic} \end{cases}. \tag{21}$$

The only missing piece here is the connection between the relative volume of the gas and our multiplicatively decomposed volume terms. To be consistent with the spherical shell mechanical surrogate for void response, the relation needed is as follows:

$$J_g = J_m \frac{\bar{J} - 1 + \varphi_o}{\varphi_o}. \tag{22}$$

5 Data Fitting

The full strain energy function is the sum of the strain energy functions introduced previously, as follows:

$$W = W_{LB} + W_D^C + W_M + W_g. \tag{23}$$

As previously mentioned, the last three volumetric strain energy terms in equation (23) supplement the first term to maintain convexity in relative volume.

The full set of model parameters that must be fit to available data is $\left\{\hat{G},\hat{K},J_b,C_{10},\varphi_o,K,p_o,\gamma\right\}$. If gas effects are negligible, as they are typically for moderate to high porosity foams deformed slowly, there are only six parameters. The contributions of each model parameter to the uniaxial strain compression response are unambiguous enough to allow good fitting to data from our tests. The process of calculating the relative volume decomposition, which is an iterative process, and the expression of the derivatives of the relative volume components with respect to the total relative volume, are presented more fully in Lewis and Rangaswamy (2015). An example fit to recently obtained uniaxial S5370 (blown PDMS foam) data is shown in Figure 8.

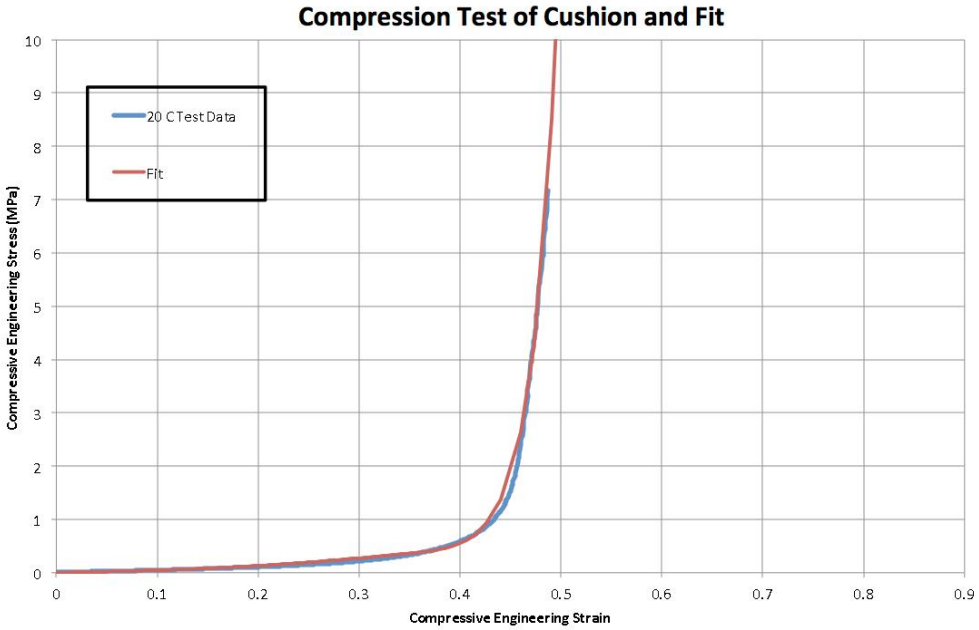

Figure 8. A model fit to recently obtained uniaxial compression data from an S5370 (blown PDMS foam) sample with a density of 0.8504 g/cc.

Note that the fitting process for the data shown in Figure 8 was somewhat simplified as the porosity of the foam was relatively low. As a result, the strain energy terms associated with low strain response in compression, namely W_{LB}, can be omitted and the parameters associated with it, namely $\hat{G}$, $\hat{K}$, and J_b, do not need to be fitted. Gas effects are negligible for the data shown in Figure 8, as the compressive strain rate was 0.01 s^{-1} and the specimen diameter was approximately 13 mm. As such, the parameters associated with W_g, namely p_o and γ do not require fitting. Additionally, the test specimen was approximately 1 mm thick, so an assumption of uniaxial strain was deemed appropriate. The only remaining parameters to fit were the porosity (ϕ_o), the parent material effective Neo-Hookean modulus (C_{10}), and the parent material effective bulk modulus (K). The fitting process consisted of looping over a range of possible porosities and using a Levenberg-Marquardt algorithm to obtain the best fits for the two moduli for each porosity, and selecting the fit associated with the porosity that had the minimum RMS error relative to the measured stress-strain curve.

6 Model Implementation

A version of the CHIPFoam model that omitted the premultiplier of J_m in the expression for J_g in equation (22) and in the modified Danielsson function in equation (18) was implemented as a UHYPER subroutine in ABAQUS. While the UHYPER framework is not as flexible for mechanical response calculation as the more general UMAT subroutine in ABAQUS, it is well suited to quick coding and testing of invariant-based hyperelastic formulations such as CHIPFoam.

The UHYPER subroutine is passed model parameter values in the PROPS array, along with any user-defined state variables in the SDV array. The implementer may update the state variables but must update the values of the energy function and its partial derivatives with respect to the first and second isochoric invariants and the relative volume up to third order. These values allow ABAQUS to calculate the Cauchy stress tensor and a

material tangent stiffness tensor to be used in calculation and iteration.

A critical part of the solution for the energy function and its derivatives is the multiplicative decomposition of J. To achieve this decomposition equation (15) was used along with equations (16), (17), (20), and (22) and a bisection algorithm. This scheme works efficiently and robustly.

7 Further work

While much work has been and much achieved in the development of CHIPFoam, much remains to be done to maximize its usefulness. The areas for further work can be grouped into topics of hyperelastic theory, dissipative behavior, and use in explicit dynamics.

In terms of hyperelastic theory development, there are three main thrusts. First, the idea of establishing a set of bulk tangent moduli at various relative volumes to best match observed lateral expansion data should be explored and the results documented. If observed low strain Poisson's effects can be matched with a few terms added to equation (10), this should be pursued. Second, the dependence of the parameters in equation (10) on porosity for a given parent material should be studied to determine whether the treatment of spatial porosity distributions mentioned in the previous section could be improved to include smaller strain dependence on porosity. Third, the inclusion of a third relative volume term in the multiplicative decomposition of J should be investigated to determine if the lack of polyconvexity that can be seen at high porosities (greater than 70%) can be removed by introducing a part of the volume change that results from buckling in the foam.

In the area of dissipative behavior, the inclusion of viscoelasticity, hysteresis, and Mullins effects should be investigated to determine the best theoretical and algorithmic treatments for modeling these phenomena. For Mullins effect approaches, we are considering the approach taken by Ogden and Roxburgh (1988) and generalized by Naumann and Ihlemann (2015) and that taken by Rickaby and Scott (2012). Once the best approaches are determined, it is likely that the model will have to be recoded as a more general UMAT to include these effects.

While this model has been implemented as a UHYPER subroutine and used for implicit, quasistatic analyses, there are reasons to apply it to explicit dynamic problems. ABAQUS/Explicit does not have an analog of the UHYPER subroutine, but has an anisotropic version that could probably be used effectively. This coding needs to be done and verified.

8 Acknowledgments

I hope it is obvious that the work in the development of this model has taken a substantial effort over several years. In reality, it has been over fifteen years in the offing. The work has been supported off and on by DOE/NNSA funding.

I am indebted to Tom Zocco and Mark Chadwick for the initial time to research this problem and develop an understanding of the RVE approach that supports the Danielsson function, along with John Dienes and Johndale Solem, whose linear elastic RVE work (Dienes and Solem, 1999) encouraged me. I also would like to thank Tom Stephens, Seth Gleiman, Jim Coons, and Rick Mooday for taking the first really compelling foam data on our elastomeric foams, and for Carl Cady and Cheng Liu for furthering this work, and having patience while we determined what data we needed. I also would like to thank Partha Rangaswamy for heading up recent test efforts and serving as a sounding board for the last several years. I would like to thank Ted Lyman for coding up the first version of CHIPFoam as a UHYPER with only a little guidance from me. Thanks also to Devin Shunk who has done the first real assembly and thermal cycle analyses with this model recently.

References

Bardenhagen, S.G., Brydon, A.D., and Guilkey, J.E., Insight into the physics of foam densification via numerical simulation, *JMPS*, 53 (2005), 597-617.

Danielsson, M., Parks, D.M., and Boyce, M.C., Constitutive modeling of porous hyperelastic materials, *Mech. of Mat.*, 36, (2004), 347-358.

Dienes, J.K. and Solem, J.C., Nonlinear behavior of some hydrostatically stressed isotropic elastomeric foams, *Acta Mech.*, 138, (1999), 155-162.

Hohe, J. and Becker, W., Effective mechanical behavior of hyperelastic honeycombs and two-dimensional model foams at finite strain, *Int J Mech Sci*, 45 (2003),891–913.

Jemiolo, S. and Turtletaub, S., Parametric model for a class of foam-like isotropic hyperelastic materials, *J. Appl. Mech.*, 67, no. 2, (2000), 248-254.

Lewis, M.W. and Rangaswamy, P., A stable hyperelastic model for foamed rubber, *Euro. Conf. on Constit. Models for Rubber VII*, Dublin, Ireland (2011), 119-124.

Lewis, M.W. and Rangaswamy, P., Toward a hyperelastic model for foamed rubber with matrix compressibility and pore gas effects, *Euro. Conf. on Constit. Models for Rubber VIII*, San Sebastian, Spain (2013), 239-244.

Lewis, M.W. and Rangaswamy, P., Volume decomposition for a robust, mechanics-based, hyperelastic foam model, *Euro. Conf. on Constit. Models for Rubber IX*, Prague, Czech Republic (2015).

Mullins, L., Effects of Stretching on the Properties of Rubber, *Rubber Chemistry and Technology*, 21, (1948), 281-300.

Naumann, C., and Ihmlemann, J., On the thermodynamics of pseudo-elastic material models which reproduce the Mullins effect, *IJSS*, 69-70 (2015), 360-369.

Ogden, R.W., Chapter 7: Elastic Properties of Solid Materials, *Non-Linear Elastic Deformations*," 1st ed., Dover Press, Mineola, New York (1984).

Ogden, R.W. and Roxburgh, D.G., A pseudo-elastic model for the Mullins effect in filled rubber, *Proc. Royal Soc. London, A: Math, Phys, and Eng Sci*, 455 (1988), 2861-2877.

Rickaby, S.R., and Scott, N.H., The Mullins effect, *Const Models for Rubber VII* (2012), CRC Press, London (2012), 273-276.

Treloar, L.R.G., *The Physics of Rubber Elasticity*, 2nd ed., Clarendon Press, Oxford (1958).

Yang, L.M., Shim, V.P.W., and Lim, C.T., A visco-hyperelastic approach to modeling the constitutive behavior of rubber, *Int J Impact Eng*, 24 (2000), 545-560.

Address: M.W. Lewis, MS A142, Los Alamos National Laboratory, Los Alamos, NM 87545
email: mlewis@lanl.gov